

## Water Conservation & Management (WCM)

DOI: http://doi.org/10.26480/wcm.02.2025.190.199



ISSN: 2523-5672 (Online) CODEN: WCMABD

RESEARCH ARTICLE

# NUMERICAL ANALYSIS OF MIXING PROCESS OF WATER AND AIR THROUGH MIXING CHAMBER USING CFD APPROACH

Abbas Fadhil Khalaf<sup>a</sup>, Farhan Lafta Rashid<sup>a,\*</sup>, Najah M. L. Al Maimuri<sup>b</sup>, Hayder I. Mohammed<sup>c</sup>, Layth Abdulameer<sup>a</sup>

- <sup>a</sup>Department of Petroleum Engineering, Engineering College, University of Kerbala, Karbala 56001, Iraq;
- <sup>b</sup>Building and Construction Techniques Engineering Department, College of Engineering and Engineering Techniques, Al-Mustaqbal University, Hillah, Babylon 51001, Iraq;
- <sup>c</sup>Department of Physics/College of Education/University of Garmian-Kurdistan region-Iraq;
- \*Corresponding Author Email: farhan.lefta@uokerbala.edu.iq

This is an open access journal distributed under the Creative Commons Attribution License CC BY 4.0, which permits unrestricted use, distribution, and reproduction in any medium, provided the original work is properly cited

#### **ARTICLE DETAILS**

#### Article History:

Received 23 November 2024 Revised 18 December 2024 Accepted 03 February 2025 Available online 16 March 2025

#### **ABSTRACT**

The mixing process of water and air is critical in various engineering applications, such as heat exchangers and atomization systems. This study numerically investigates the thermal and velocity distributions in a water-air mixing chamber using the Computational Fluid Dynamics (CFD) approach in ANSYS/FLUENT 16. The objective is to analyze how different inlet velocities influence temperature distribution and mixing efficiency to optimize thermal management in industrial applications. Numerical simulations were conducted for various inlet velocity pairs, including (V1 = 0.1 m/s, V2 = 0.1 m/s) and (V1 = 0.5 m/s, V2 = 0.1 m/s). The results indicate that increasing the inlet velocity of water enhances heat transfer efficiency. For instance, at point 1, the temperature increased from 298 K to 300 K for V1 = 0.1 m/s and V2 = 0.1 m/s, while it rose from 335 K to 330 K when V1 was 0.5 m/s. Similarly, at point 2, the temperature improved from 296 K to 302 K for higher air velocities, highlighting better thermal mixing. Velocity distributions further confirmed that higher air velocities promoted more uniform mixing patterns within the chamber. The findings emphasize that inlet velocities significantly affect temperature uniformity and mixing efficiency, providing insights for optimizing heat transfer in industrial fluid systems. This research lays the foundation for further investigations into fluid coupling mechanisms and advanced thermal control strategies.

#### **KEYWORDS**

 ${\bf Mixing\ process, Mixing\ chamber, ANSYS\ fluent, Engineering\ applications, CFD\ approach.}$ 

#### 1. Introduction

The interaction between liquids and gases in industrial processes requires precise engineering to attain desired results. An important application is the atomisation of liquids into small droplets or sprays in gaseous environments (Vojkůvková, et al., 2015). This phenomenon supports several applications, including combustion, spray painting, chemical manufacture, agricultural irrigation, and medicine delivery systems. The idea of atomisation is fundamental to these applications, profoundly influencing performance parameters such as droplet size, dispersion, and velocity. Various atomisation methods, including effervescent atomisers, have been created to optimise these characteristics (Abbas Fadhil, et al., 2024; Sliusenko, et al., 2021).

Gas added to a liquid to make a bubbly flow is termed effervescent atomisation; it is a type of dual fluid atomisation. The procedure involves the injection of specific velocities of gas into the liquid phase and the creation of bubbles which expand once they leave the nozzle (Sheha, et al., 2024). Such expansion leads to pressure drop; the liquid breaks into narrow streams and droplets that are minute in size (Lefebvre, et al., 1988), in the 1980s, designed effervescent atomisers with remarkable advantages over the original atomisers, including high atomisation efficiency at low-pressure gas, minimum gas use, and capability in handling contaminated liquids due to the larger nozzle diameter. In addition, it has fuelled the need to aerate liquid fuels to enhance combustion efficiency and

reduce NOx emissions. Despite their advantages, several aspects of their internal operations with effervescent atomisers are not yet well understood. T) the two-phase flow pattern in these devices is important for lean and spry characteristics and atomiser efficiency. The changeover between slug and annular flow regimes in the mixing chamber is critical in determining the droplet size and spray dispersion. Many experimental and computational studies have attempted to explain these dynamics (Shao et al., 2021; Ferreira et al., 2009).

The recent findings, therefore, reveal that numerical solutions, and in particular computational fluid dynamics (CFD), have emerged as useful tools for modelling and visualizing the internal flow characteristics of effervescent atomisers. In order to mimic the flow field of a V-type aeratedliquid injector, carried out two and three-dimensional computations with the help of a mixture model (Tian et al., 2003). These predictions, supported by experimental data, paid special attention to the transition from a slug and annular flow depending on the gas-to-liquid mass ratio GLR. In the subsequent study, Esfarjani and Dolatabadi utilized the Multi-Fluid Marker and Cell (MFMAC) approach to understand the behavior of the liquid films carrying nanoparticles when different aeration is being used (Esfarjani et al., 2009). According to their conclusions, improved aeration promotes mixing and helps transition from slug to annular flow. Mehmood and Masud used the Volume of Fluid (VOF) technique to simulate internal flow phenomena in a more realistic tri-dimensional configuration, and the results obtained were in concordance with the

**Quick Response Code** 

Access this article online



Website: www.watconman.org DOI:

10.26480/wcm.02.2025.190.199

previous research (Mehmood and Masud, 2012).

Besides atomisers, jet pumps are the second vital component that is used strongly in fluid mixing in various industries, such as petroleum, metallurgical, and refrigeration (Devos et al., 2025). While rotary pumps are comparatively more complex and require frequent replacement of mechanical seals, jet pumps use fluid dynamics instead, and this offers such advantages as it is quite easy and reliable, and the cost of their maintenance is almost negligible. As in atomizers, the mixing chamber in jet pumps is vital for performance definition. CFJP and CAJP have been studied previously with idealisation of their mixing characteristics (Jing et al., 2022).

Recent advancements in the design of jet pumps have focused on procedures to introduce a self-sustained oscillation mechanism in the mixing chamber. This invention enhances the efficient blending of the fluids and ultimately improves the efficiency of the pumps in general. The studies shown pointed out that self-excited oscillations produce advective pressure zones, thus enhancing sufficient mixing and increasing the capacity of jets. Still, there remains the question of additional enhancements that are needed for the geometrical characteristics and working parameters of the jet pumps in order to achieve the most effective mixing by (Li et al., 2007; Wang et al., 2011). conducted research on the enhancement of the axial stream of the jet pump by using a novel design for the blending chamber in addition to a regulated intake swirl (Sheha et al., 2024). They discovered that the creation of a swirl in the suction chamber results in a 12.76% increase in pump efficiency when compared to the identical pump design that does not include a swirl. According to the findings who investigated the impact of hybrid coaxial air and hydrogen jets on fuel mixing at supersonic crossflow, they discovered that the injection of coaxial air and fuel jets at supersonic crossflow considerably increases the fuel penetration and mixing that occurs inside the combustion chamber of (Zhang et al., 2021).

Despite extensive research on fluid mixing and atomization, significant gaps remain in understanding the interaction between water and air at varying inlet velocities, particularly within controlled mixing chambers. Previous studies have primarily focused on either single-phase flow dynamics or specific geometric designs, often overlooking the combined effects of velocity variations on thermal and velocity distributions. The motivation for this research stems from the need to enhance heat transfer efficiency in industrial fluid systems, where optimal thermal management is crucial for energy savings and system performance. This study innovates by employing a computational approach to analyze the cumulative impact of different inlet velocity pairs on temperature uniformity and mixing behavior, providing a more comprehensive understanding of fluid coupling mechanisms. The findings offer valuable insights for designing more efficient thermal management systems in applications such as heat exchangers, chemical processing, and environmental control. By addressing these critical gaps, this work contributes to the advancement of engineering solutions for improved fluid mixing performance.

### 2. PROBLEM DESCRIPTION AND MATHEMATICAL FORMULATION

In this section, the fundamental issues regarding the mixing process of water and air are described; it is suggested that engineering students ought to have a clear concept of fluid mechanics for solving problems related to the mixing process. The research mainly centers on the interference of the two disparate air and water phases at different flow conditions, with varying velocities of V1 and V2. The components include the ultimate energy, discharge, and development equations used in the simulation of the behaving fluid during blending. The solutions to these equations are obtained using the finite volume method on ANSYS/FLUENT software to realize the new flow features and temperature fields. In this process, the formulation also includes the boundary and initial conditions relevant to the current experimentation to synchronize the numerical model and the physical process of mixing. This approach is done to assess better the ability of blending and thermal convection between the two fluids and, in turn, improve designs in various engineering disciplines.

In the study, the placement of the device was geometrically explained, and to illustrate the geometry of the mixing chamber where water and air interact, Figure (1) shows the schematic roadmap of the device at the mixing chamber. The diagram offered has particular tested points, designated as (1, 2, 3, 4), which are lodged interfering with the distributions of temperature and velocity at the time of the mixing phase. The flow properties of the fluids are assumed to be water at an inlet temperature of 330 K and air at 300 K, while the inlet velocities are varied as V1 and V2 in order to understand the impact of these parameters on the

performance of the mixing in the present system. This configuration is used for flow detection, and thermal integration is incorporated in the construction of this device, making it easy to sketch the experiment layout using the numerical flow.

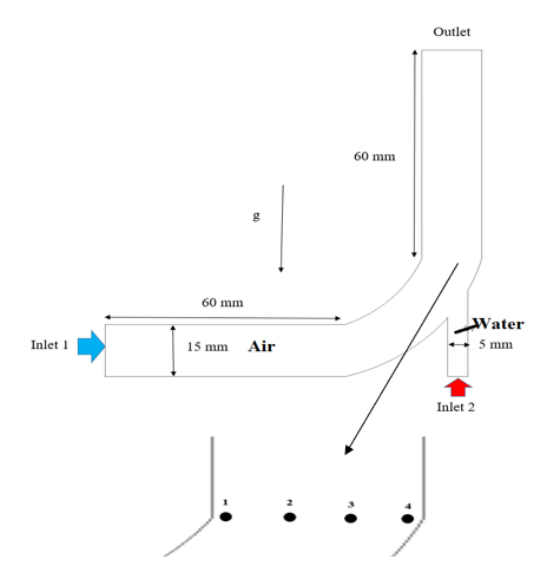


**Figure 1:** A schematic diagram showing the geometry of the device and tested points

#### 2.1 Governing equations

The numerical analysis gives the ability to predict details of the mixing process of water with air in a mixer chamber. It was determined that the flow was two-dimensional, incompressible, and unstable. Continuity, momentum, and energy equations are used to simulate this process as presented in (1), (2), and (3), respectively (Rashid et al., 2024; . Al-Naggash et al., 2024; Khalaf et al., 2024):

$$\partial \rho / \partial t + \nabla \left( \rho . V \right) = 0 \tag{1}$$

$$\partial (\rho v)\partial t + \nabla (\rho V) = -\nabla P + \mu \nabla 2V + \rho g + S \tag{2}$$

$$\partial/\partial t (\rho.H) + \nabla (\rho.V.H) = \nabla.(K.\nabla T)$$
 (3)

## 2.2 Materials

Table 1 provides the thermophysical characteristics of the working media used in the research, namely air and water, determining their behaviour when mixing. Among the properties enumerated are density, specific heat, thermal conductivity, and viscosity. These are important for modelling the fluid dynamics and the thermal couplings incorporated in the numerical simulations performed within the ANSYS/FLUENT environment.

Table 1: Thermophysical proprieties of the used materials		
Properties	Air	water
Viscosity (kg/m-s)	0.0000178	0.001003
Thermal conductivity (W/m-k)	0.0242	0.6
specific heat (J/kg-k)	1006.43	4182
Density (kg/m³)	1.225	998.2

The configuration of the mesh model employed in the numerical simulations of the mixing process of water and air is shown in Figure (2). This implies that the mesh is purposely intended to divide the computational domain to adequately describe the flow of fluids and their thermal relationship within the mixing chamber. The configuration comprises a pre-established structured grid so that an adequate resolution is achievable in areas with high gradients, such as near the inlet and within the mixing zone, to capture the flow features realistically. The quality and density of the mesh are the most important parameters for getting closer results to the actual simulation. The Figure shows the mesh density and distribution of the grids, neglecting mesh dependence during simulation computation.

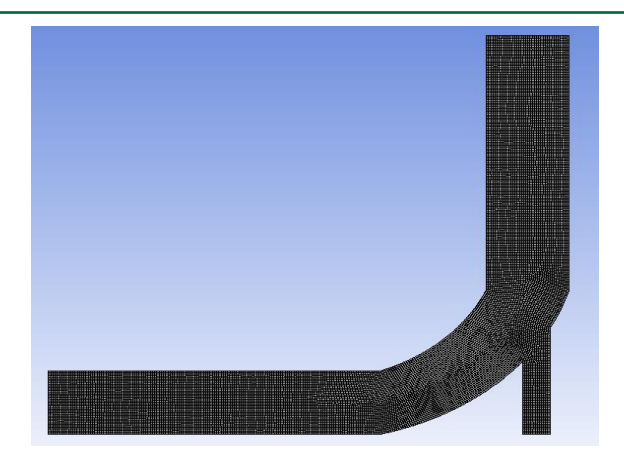


Figure 2: Configuration of mesh model

#### 2.4. Grid independence and the code validation tests

The independence test for the independent grid and the numerical code validation test were carried out to verify the numerical simulations. To perform the grid independence, several mesh densities were tried, and the results reveal that for the current CFD simulation, 5.57 million nodes are adequate to give results with minimal fluctuation in the output parameters of the work, like temperature and velocity distributions while performing the grid independence test. For example, mesh sizes of 23657, 25678, 28976, and 31879 elements were used to conduct simulations, and the analysis showed that the results were relatively stable at 28976 elements, making the resolution adequate (figure (3).

Figure 4 presents the current numerical model by comparing its outcomes with the experimental findings of Bahatkar and Sur (Bhatkar and Sur, 2021). The model is utilised with identical geometry in their tests, facilitating a direct comparison. The flow ratio demonstrates strong concordance, with both computational and experimental findings exhibiting a comparable trend, attaining about 2.5 at an input of 0.5. Minor discrepancies are noted in the pressure ratio and efficiency, with a maximum error of around 15%, presumably attributable to experimental errors or modelling assumptions. Notwithstanding these tiny discrepancies, the overarching patterns correspond closely, validating the model's precision. This validation confirms the numerical model's dependability in reproducing experimental results and its appropriateness for evaluating ejector performance under diverse settings, establishing it as a robust instrument for further research in this field.

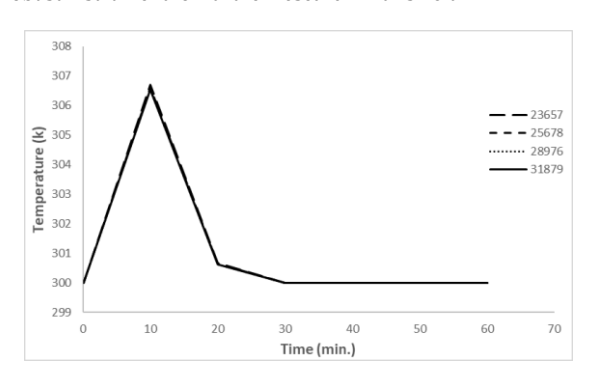
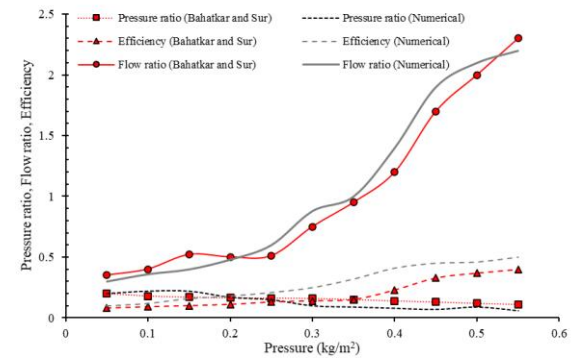


Figure 3: Grid independence test for V1=0.1, V2=0.1 m/s at point 1



**Figure 4:** Comparison of numerical simulation and results of experimental work of Bahatkar and Sur (Bhatkar, and Sur, 2021)

#### 3. RESULTS AND DISCUSSION

#### 3.1. Case one (V1=0.1, V2=0.1 m/s)

The temperature distribution of the fluid at different time intervals when inlet velocities are V1 = 0.1 m/s and V2 = 0.1 m/s is demonstrated in Figure (5) in the form of a temperature contour plot. The integration of temperature distribution shows that the water at 330K gradually blends with the air at 300K in the mixing chamber, and hence, a temperature differential exists across the mixing chamber. At 0 minutes, the positive regions of the contours delineate the initial clear interface between the two fluids with water at a higher temperature. For the outline of the contours, they depict a relatively spread-out temperature that rises to about 305 K at 10 minutes and stabilizes at 302 K for the next 30 minutes.

As shown in Figure (6), the concentrations of velocity distribution at different time intervals regarding the mixing chamber have been depicted for the case where the inlet velocities were V1 = 0.1 m/s and V2 = 0.1 m/s. For the initial analysis, at 0 minutes, the velocity contour plotted in Figure 3 shows a nearly steady flow pattern near the inlet area with the maximum velocity reaching up to 0.1 m/s. At 10 minutes, with the help of the contours, a bit more advanced flow structure is seen as a consequence of the interaction of the incoming water and air streams to form regions of higher velocities. At a later point, 30 min later, the velocity distribution becomes relatively steady, and the flow is more uniform, with the velocities ranging around a mean of 0.08 m/s throughout the chamber.

Figure (7) illustrates the temperature at points 1, 2, 3 and 4 in the mixing chamber for inlet velocities of V1=0.1m/s and V2= 0.1m/s. The temperature analysis at these points shows that they have different thermal histories. At the starting instant (t=0 min), the hottest point, 1 near the water inlet, measures 330 K, while the lowest point, measuring only 300 K, is near the air inlet point 4. When time counts on 10 minutes, the temperature record of point 1 is reduced to 320 K, while the record of point 4 increases approximately to 305 K, proving saving of heat. At 30 minutes, the temperature log from points 2 and 3, midway between the inlets, stands at 310 K and 308 K, respectively.

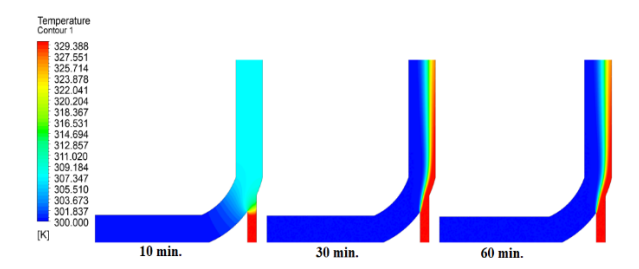
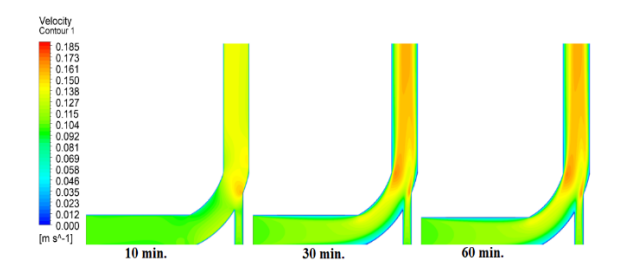
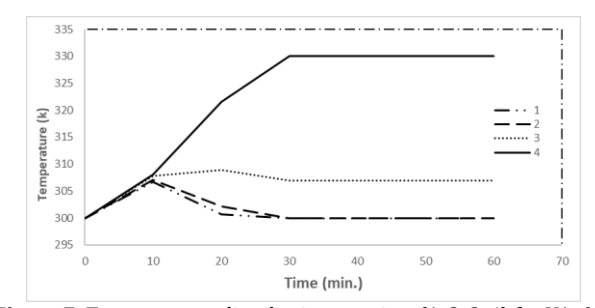


Figure 5: Contours of temperature distribution for V1=0.1, V2=0.1 m/s at different times.



**Figure 6:** Contours of velocity distribution for V1=0.1, V2=0.1 m/s at different times.



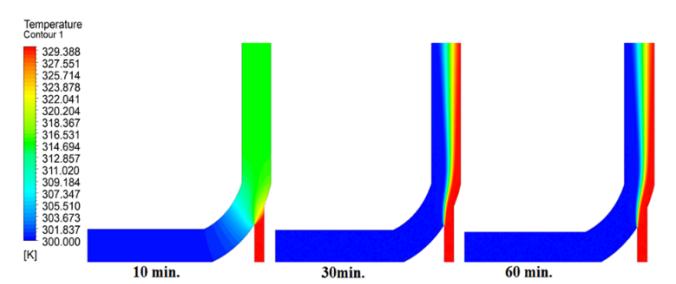
**Figure 7:** Temperatures distribution at points (1, 2, 3, 4) for V1=0.1, V2=0.1 m/s

#### 3.2. Case two (V1=0.1, V2=0.3 m/s)

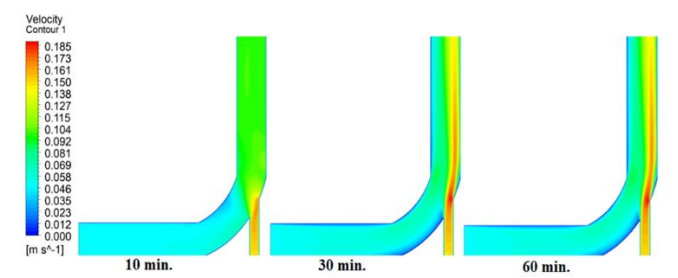
Figure (8) refers to the present case with inlet velocities of V1 = 0.1 m/s and V2 = 0.3 m/s and provides insight into the mixing chamber's temperature distribution over various time instants. In the first frame at t=0 minutes, the isotherms depict a warm water phase at approximately 330 K and a cold air phase at about 295 K. At the time of 10 minutes, the contours reveal a better-mixed zone as depicted in the temperature profile of the water inlet at about 320K and the air at about 300K. Up to 30 minutes, the temperature distribution becomes smoothed with normalized values of approximately 310 K in the center of the chamber, which is associated with the higher air stream velocity and results in better mixing.

Figure (9) depicts the velocity distribution of the flow situation inside the mixing chamber for the flow rates of V1 = 0.1 m/s and V2 = 0.3 m/s concerning the flow characteristics at specific time instances. For the initial time at 0 minutes, the velocity contours indicate a reasonably uniform flow distribution within the tunnel but with the highest velocities recorded near the air inlet about 0.3 m/s and water inlet velocity of about 0.1 m/s. At 10 minutes, the contours begin to depict a richer flow structure within the chamber, with velocities increasing in the central regions of the chamber as the two streams start to interact. At 30 minutes, the velocity profile stabilizes, and the average velocity range from 0.25m/s indicates good mixing and a faster flow rate at the mid-section.

In the case of inlet velocities of V1 = 0.1 m/s and V2 = 0.3 m/s, the temperature distribution of the flow at particular points in the mixing chamber is shown in Figure (10). A temperature of about 330 K is observed at point 1, close to the water inlet, at 0 minutes; at the same time, point 4, near the air inlet, has a temperature of about 295 K. When the simulation moves on to 10 minutes, the temperature at point 1 is about 320 K, which shows a cooling effect when an explosion occurs, the temperature of point 4 increases to approximately 302 K, caused by the warm water interacting with the cold air. At 30 minutes into the experiment, we get to temperatures of approximately 310 K for point 2, located between point 2 and point 3, and approximately 308 K for point 3, which is also between the two inlets.



**Figure 8:** Contours of temperature distribution for V1=0.1, V2=0.3 m/s at different times.



**Figure 9:** Contours of velocity distribution for V1=0.1, V2=0.3 m/s at different times.

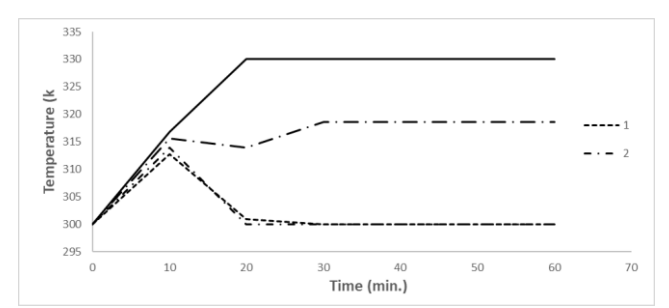


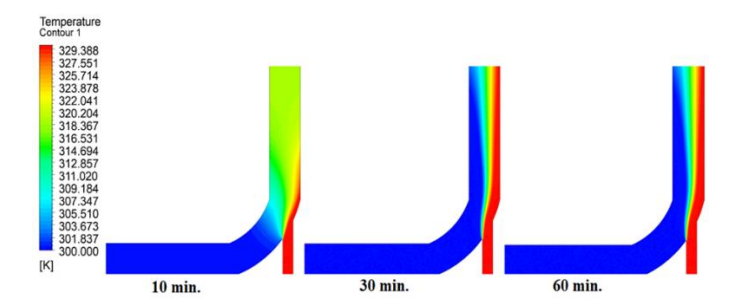
Figure 10: Temperatures distribution at points (1, 2, 3, 4) for V1=0.1, V2=0.3 m/s

#### 3.3. Case three (V1=0.1, V2=0.5 m/s)

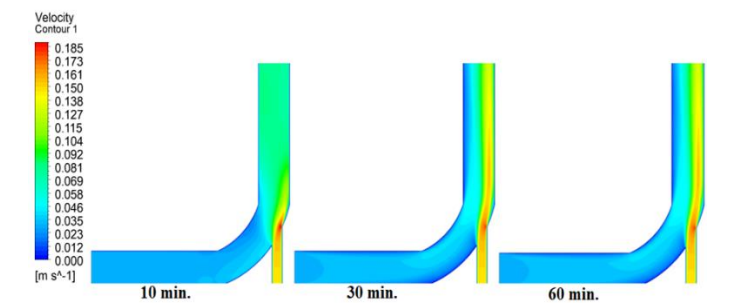
Fig. (11) depicts the temperature distribution of the present phase for the inlet velocities of V1 = 0.1 m/s and V2 = 0.5 m/s and indicates the thermal characteristics of the mixing chamber at specific time steps. At the beginning of the process (0 minutes), the isotherms indicate temperature stratification: the inlet water temperature is approximately 330 K, and the inlet air temperature is near 295 K. At 10 min, the temperature at the water inlet of the cooling jacket is about 320 K, and the air temperature is about 305 K, therefore implying effective heat transfer had taken place. At 30 minutes, the temperature of the computational domain is more or less equally distributed; the temperature reaches 312 K for point 2 and 310 K for point 3. This is because the higher air inlet velocity of 0.5 m/s improves the mixing process, hence the quick attainment of thermal balance and higher temperature penetration across the chamber than in the other cases.

Figure (12) displays velocity distribution contour plots for the problem with different inlet velocities of v1= 0.1~m/s and v2 = 0.3~m/s at specific time steps. As seen at the start time, t=0 mins, there is a substantial disparity in the velocity contour, with the variation of maximum velocity distinct near the air inlet at 0.3~m/s while that of maximum water inlet velocity at 0.1~m/s. At 10 minutes, the shapes suggest a more elaborated movement pattern, with higher velocities in the central core of the chamber due to the merging of the two fluids. The velocities at other zones gradually decrease, confirming adequate mixing in the centre area by 0.30~and a sustained higher average velocity of 0.25~m/s.

The temperature distribution at different points (1, 2, 3 and 4) in the mixing chamber for the case of inlet velocities V1=0.1m/s and V2=0.5 m/s has been shown in Figure (13). The temperature near the water inlet at 0 minutes is close to point 1 at about 33 °C = 306 K, whereas that near the air inlet, point 4, is 26.67 °C = 300 K. At 10 minutes, point 1 drops to nearly 320 K by the cooling impact of the mix while point 4 increases to almost 302 K with the influence of warm water with cold air. Temperature values at points 2 and 3 between the inlets rise to 315 K and 312 K at 30 min. The analysis of this data suggests that, in particular, the increase in velocity of air supplied to the inlet section to 0.5 m/s contributes to more efficient penetration and mixing of this gas phase with the other materials across the chamber volume, contributing to faster establishment of thermal equilibrium across the chamber and more uniform temperature distribution, as compared to cases with the lower inlet velocities.



**Figure 11:** Contours of temperature distribution for V1=0.1, V2=0.5 m/s at different time.



**Figure 12:** Contours of velocity distribution for V1=0.1, V2=0.3 m/s at different times.

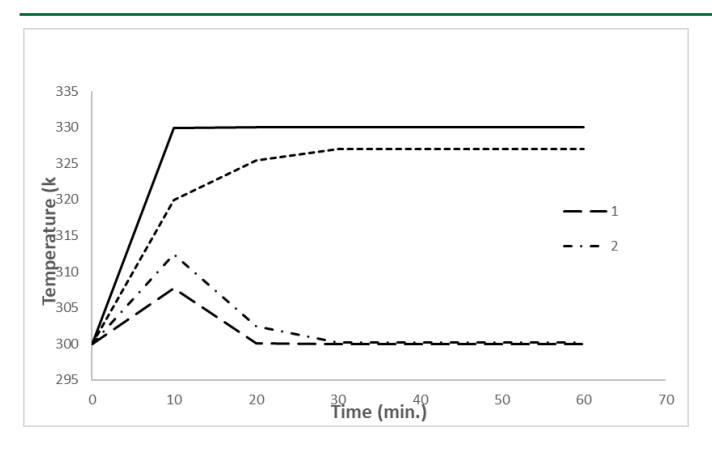


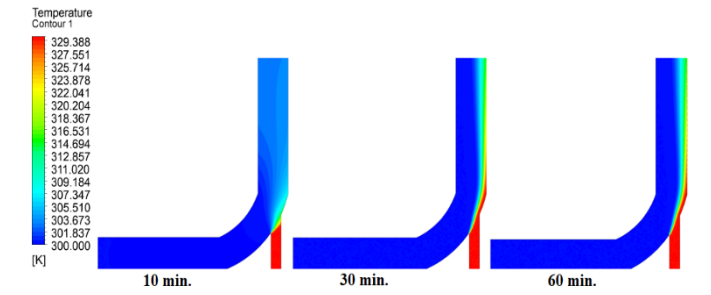
Figure 13: Temperatures distribution at points (1, 2, 3, 4) for V1=0.1, V2=0.5 m/s

#### 3.4. Case four (V1=0.3, V2=0.1 m/s)

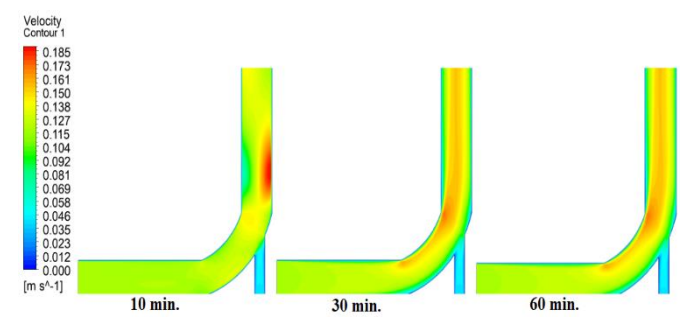
Temperature distribution contours are presented in Fig. (14) for the flow inlet velocities V1 = 0.3 m/s and V2 = 0.1 m/s at definite time steps. Starting with the temperature history at the first time equal to 0 minutes, the temperature of point 1, which corresponds to the water inlet temperature, is equal to 330 K, whereas the air inlet temperature at point 4 is 295 K. At 10 minutes, point 1 reduces to about 325 K revealing a little heat loss as point 4 increases to about 300 K due to the addition of warm water to the cold air. The calmer temperature of about 310 K and 308 K at points 2 and 3 is reached 30 minutes after the inlet mixing.

Figure (15) shows the velocity range for velocity streamlines at the inlet velocities of V1 = 0.3 m/s and V2 = 0.1 m/s at different time instants. As observed in the first instance, when time=0 minutes, the velocity near the water inlet stands at 0.3 m/s while the velocity near the air inlet is 0.1 m/s. At a time of 10 min, the positional map also demonstrates a more clearly expressed flow structure; there is a weak flow in the central part of the chamber with a velocity of approximately 0.2 m/s against the background of the slow-down zone. At thirty minutes, the velocity in the central area is about 0.15 m/s, which shows that the lower air inlet's velocity negatively impacts the mixing efficiency. This causes the flow regime to be less oscillatory, with velocity distribution remaining low and non-uniform, especially in the vicinity of the air inlet opening.

Figure (16) depicts the case's temperature variation at particular sections (1, 2, 3 and 4) with the velocities V1 = 0.3 m/s and V2 = 0.1 m/s. The temperature data at the first time 0 minutes are as follows: point 1, near the water inlet, is approximately 330 K, and point 4, near the air inlet, is approximately 295 K. At 10 minutes, point 1 cools to slightly below 325 K and point 4 increases to about 298 K because the warm water now mixes with the cooler air. At 30 minutes, points 2 and 3 between two inlets maintain temperatures of 310 K and 308 K, respectively. This data proves that the increase in a water inlet velocity of 0.3 m/s is great for heat transfer, but the air inlet velocity of 0.1 m/s is ineffective for mixing. Therefore, the thermal distribution is still non-uniform, characterized by a temperature gradient between water flow and air, emphasizing the necessity to control inlet velocities to obtain a more uniform temperature distribution in the mixing chamber.



**Figure 14:** Contours of temperature distribution for V1=0.3, V2=0.1 m/s at different times.



**Figure 15:** Contours of velocity distribution for V1=0.3, V2=0.1 m/s at different time.

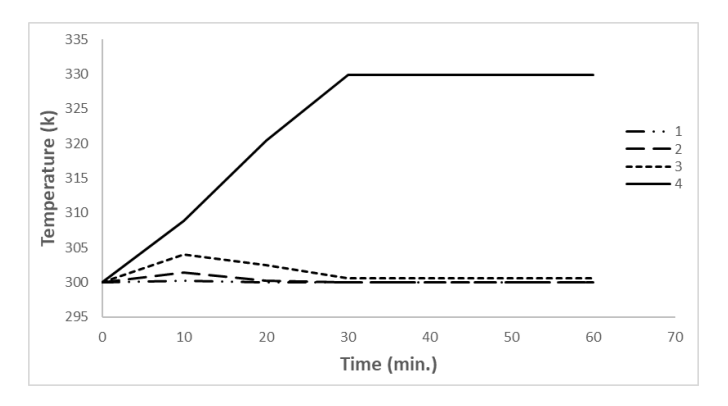


**Figure 16**: Temperatures distribution at points (1, 2, 3, 4) for V1=0.3, V2=0.1 m/s

#### 3.5. Case four (V1=0.5, V2=0.1 m/s)

Figure (17) illustrates the temperature contours distribution for the case with inlet velocities of V1 = 0.5 m/s and V2 = 0.1 m/s at different time steps. I show that at the first time step (t= 0 minutes), the system's highest temperature, about 335 K, is recorded at point 1 near the water inlet, and the lowest temperature of about 295 K at point 4 near the air inlet. At 10 minutes, the point is lowered to about 330K, showing heat loss, and point 4 increases to roughly 300 K because water mixes with warm air. At 30 minutes, points 2 and 3 between the inlets dictate 315 K and 312 K temperature, respectively. The temperature distribution of this water flow rate of 0.5m/s shows that this inlet velocity enhances the mixing efficiency of water in the chamber, thereby allowing faster attaining of thermal equilibrium. Again, there is evidence of better thermal distribution in comparison with cases where lower water velocities were used, which proves the efficiency of the enhanced water flow rate in providing better thermal convection and thus obtaining a more homogeneous temperature distribution across the tested facility.

Figure (18) presents the line-type representation of the velocity distribution contour for the case with inlet velocities of V1 = 0.5 m/s and V2 = 0.1 m/s at different time intervals. The velocity near the water inlet (point 1 at t = 0 min) was approximately 0.5 m/s, and the air inlet (point 4, t = 0 min) was about 0.1 m/s. After the time goes to 10 minutes, velocity in the central part of the chamber reduces to 0.35m/s, demonstrating the impact of the slow-moving air in the general flow. At 30 minutes, the average velocity in the central location returns to 0.25 m/s; this shows that while water inlet velocity increases, low air inlet velocity reduces the overall mixing efficiency. The flow boundaries also highlight a steep velocity gradient with more incredible velocity, leading to a more complex flow field than the slower-moving air stream, causing velocity variations that are not as uniformly distributed over the cross-section.

The temperature profile for points 1, 2, 3, and 4 for the case of inlet velocities is shown in figure (19) for V1 0.5 m/s and V2 = 0.1 m/s. Point 1, which is close to the wall with a water inlet at time = 0 min, records a temperature of about 335 K, while point 4, which is close to the wall with an air inlet, records a much lower temperature of about 295 K. When moving to the tenth minute, the temperature of the first point is 330 K, which means that it has cooled somewhat, and the temperature of the fourth point is 300 K due to water warming. After 30 minutes, the temperatures of points 2 and 3, located between two inlets, correspondingly range from 320 K to 315 K. A steady rise of temperature at the cooler points by the associated case corresponds to the improved heat transfer as predicted by the data for the water inlet velocity of 0.5 m/s as compared to the water velocities in the lower range.

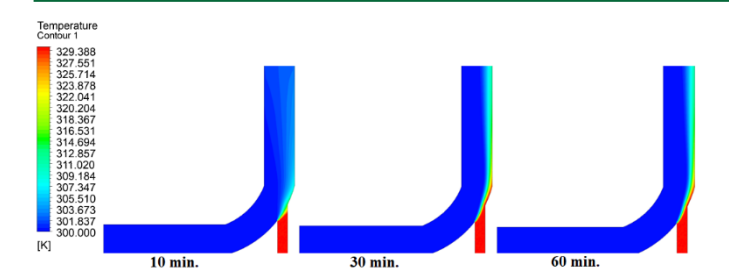
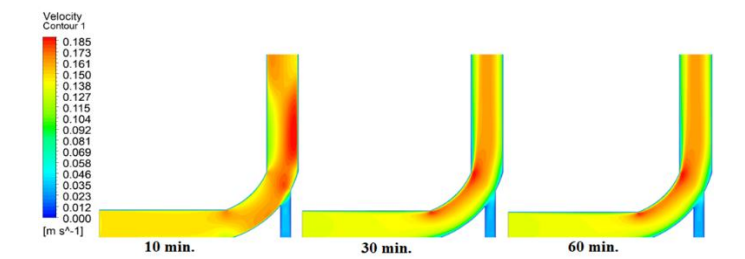


Figure 17: Contours of temperature distribution for V1=0.5, V2=0.1 m/s at different times



**Figure 18:** Contours of velocity distribution for V1=0.5, V2=0.1 m/s at different times.

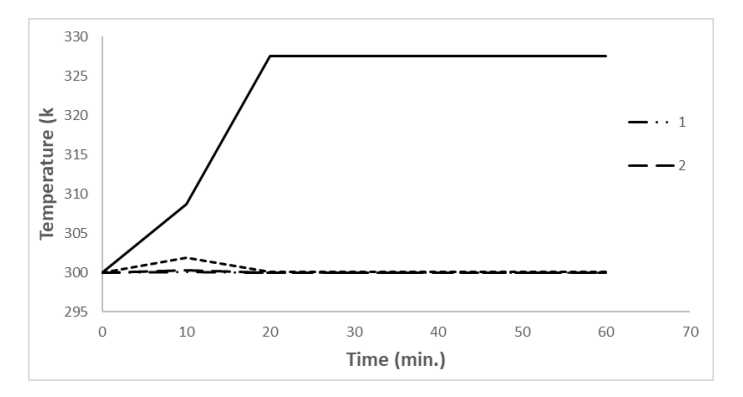


Figure 19: Temperatures distribution at points (1, 2, 3, 4) for V1=0.5, V2=0.1 m/s.

## 3.6 Compression of all cases

Figure (20) reveals the variation in local temperature for the four cases: V1 = 0.1 m/s and V2 = 0.3 m/s and V1 = 0.3 m/s and V2 = 0.1 m/s. In the first case, V1 = 0.1, V2 = 0.3 m/s, it can be seen that the temperature at point 1 near the water inlet begins from around 298K and by the end of 30 minutes reaches 305 K, which is an increase, though gradual due to increased air velocity which led to some mixing. Compared with the first case (V1 = 0.3, V2 = 0.1 m/s), point 1 starts with a higher temperature of about 310 K and reaches a stable temperature of about 315 K after the same time as well as the more effective heat transfer from the water due to the increased velocity of the water. The comparison showed that even though both configurations cause the temperature to rise, the system with the higher water inlet velocity (V1 = 0.3 m/s) experiences a more dramatic temperature change and a faster rate, proving the paramount importance of inlet velocities as factors affecting the thermal distribution and mixtures efficiency in the system.

Figure (21) compares temperature distribution for two cases: Thus, we obtain the pair V1 = 0.1 m/s, V2 = 0.5 m/s versus V1 = 0.5 m/s and V2 = 0.1 m/s. In the first case (V1 = 0.1, V2 = 0.5 m/s), the temperature at point 1, near the water inlet, increases slowly from 295 Kelvin up to 300 Kelvin after 30 minutes. On the other hand, in the second case (V1 = 0.5, V2 = 0.1 m/s), point 1 starts at a higher temperature of about 335 K and ends at nearly 330 K after the same time – the illustration of the higher rate of water inlet velocity at enhancing heat transfer. The same trend can be seen at point 4, close to the air inlet, although the temperature increase in the first case is less than in the second. This comparison shows how water velocity is pivotal in the ability of a system to achieve ideal thermal mixing and tie the varied areas in the system to a similar temperature, which was made evident by the higher heat transfer rate and shorter time needed to reach thermal equilibrium in the system as a result of the higher water flow rate.

Figure (22) illustrates the comparison of velocity distribution for two cases: In the case where V1 = 0.1 m/s and V2 = 0.3 m/s as well as when V1 = 0.3 m/s and V2 = 0.1 m/s. In the first case, it is shown that at point 1 near the water inlet, the velocity is about 0.1 m/s initially; thus, the flow rate through the system is quite low. Over time, the velocity permutation at point 4, near the air inlet, achieves around 0.25 m/s, suggesting an inflexion from the faster airflow. On the other hand, the second case with V1 = 0.3 m/s and V2 = 0.1 m/s depicts the first velocity streamline higher than that of the second, about 0.3 m/s; hence, the flow pattern is more distinct. At the end of the observation period, velocities at point 4 are still low at about 0.1 m/s, although the general flow characteristics are more stable owing to the higher water inlet velocity. This comparison amply illustrates how the difference in inlet velocity can also lead to enormously different patterns of velocity distribution within the system: on balance, the faster water flow in the second case was the likely reason the internal convective environment was more stirred and thus affected the thermal conditions

Figure (23) compares the velocity distribution for two cases: As another example, we had two velocities of 0.1 m/s for V1 and 0.5 m/s for V2 compared to two velocities in which V1 was 0.5 m/s and V2 was 0.1 m/s. For the first simulation set (V1 = 0.1, V2 = 0.5 m/s), point 1, close to the water inlet velocity, is around 0.1m/s while point 4, close to the air inlet velocity, is higher and approx. 0.45 m/s due to massive airflow. This is why this configuration of jets creates a relatively low overall flow rate whose mixing efficacy may be inadequate. However, the second case will demonstrate a higher initial velocity mode at point one of about 0.5 m/s, leading to active flow throughout the system. As we also notice at the end of the observation period, the velocity at point 4 is still relatively low at about 0.1 m/s; however, the increased flow of water from the reaction chamber boosts the circulation of velocities within the chamber. This comparison also sheds light on the role of inlet velocities in the flow characteristics because the second case operates at the higher water velocity that arguably enhances mixing and, consequently, the system's thermal performance.

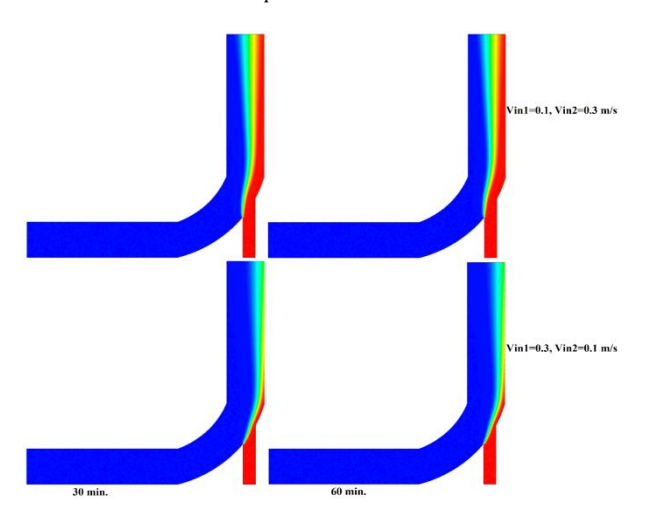
Figure (24) compares the temperature distribution at point 1 for other cases, particularly for different inlet velocities. In the case with V1 = 0.1 m/s and V2 = 0.1 m/s, the temperature profile reveals that it increases slowly from 298 K to 300 K in half an hour, which supports the above hypothesis. Following the values in Table 2 for V1 = 0.1 m/s and V2 = 0.3m/s, the temperature at point 1 starts at nearly 299K and reaches around 305 K, as the heat transfer is even more effective than in previous simulations. However, when the velocity of the water at the first point is set at 0.5 m/s and the second point is set at 0.1 m/s, we observe that temperature at point 1 starts at about 335 K and gradually drops to about 330 K after some time which clearly shows the effect of water velocity in thermal distribution. Lastly, at point 1 at V1 = 0.1 m/s and V2 = 0.5 m/s, the temperature too rises from 295 K to 300 K. Shown from the distribution presented above is the capability, demonstrated through the disparity of flow rates at the inlet in velocity of the water, to manipulate and improve thermal performance within the system by raising the velocity more rapidly and to higher temperatures at point 1.

Figure (25) compares the temperature field where x = 2, showing the effect of inlet velocity variation on thermal conditions. When V1 is considered to be 0.1 m/s and V2 0.1 m/s, it is ascertained that the temperature at point 2 initiates at nearly 295 K and rises to about 298 K in 30 mins, revealing that the heat transfer is very nominal. When linear velocities at points V1 and V2 are equal to 0.1 m/s and 0.3 m/s, respectively, then the temperature is at a starting point of about 296 K and reaches almost 302 K, which indicates an enhancement of thermal processes in the presence of airflow velocity. On the other hand, if taking the case when V1 = 0.5 m/s and V2 = 0.1 m/s, the temperature difference is higher, being about 335K initially and approximately 330 K subsequently, due to a higher magnitude of velocity of water to improve heat transfer. Finally, for the inflow velocity equal to V1 = 0.1 m/s and outflow velocity equal to V2 = 0.5 m/s, the temperature at point 2 is initially equal to 295 K and towards the end it equals to approximately 300 K, which can be characterized as moderate augmentation. This comparison demonstrates that water velocities through the inlet play a significant role in determining temperature profiles, with higher velocities achieving better heat conduction and time to reach a steady state at point 2.

Figure (26) shows the temperature variation for point 3 by varying the inlet velocities, which simulate the swirl combustor's thermal behaviors. According to the numerical analysis Table 1, when V1 = 0.1 m/s and V2 = 0.1 m/s, the temperature at point 3 at the initial time is about 295K and at the final time, which after the observation period, is nearly 298K, which shows that heat transfer is not so efficient. For case twelve, with V1 = 0.1

m/s and V2 = 0.3 m/s, the temperature in point 3 starts from nearly 296 K and increases to 303 K; it is again shown that the heat transfer is more effective at the higher air velocity. Namely, for the conditions diagnosed with V1 = 0.5 m/s and V2 = 0.1 m/s, the temperature at point 3 increases significantly and oscillates in the region of 335 to 330 K, indicating higher thermal activity of the system due to higher water flow velocity. Finally, when V1 = 0.1 m/s and V2 = 0.5 m/s, the temperature at the third node rises from 295 K to about 301 K and, therefore, experiences a relatively small rise; this comparison also highlights how inlet velocities can significantly affect temperature distribution at point 3 when higher flow rates of water enhance heat transfer and thermal equilibrium times.

The temperature distribution at point 4 is depicted for the different inlet velocities in Figure (27) to discuss the flow rate effects on thermal characteristics. When V1 = 0.1 m/s and V2 = 0.1 m/s, the temperature distribution across point 4 at the start is about 295 K, and after 30 minutes, it rises slightly to 298 K, thus proving that there was a poor heat transfer rate as a result of low velocity. If V1 is set at 0.1 m/s and V2 is set to 0.3 m/s, there will be an increase in the temperature noted at point 4, commencing from 296 K and rising to around 302 K, which signifies better thermal efficiency. On the other hand, the case with V1 = 0.5 m/s and V2 =0.1 m/s has a higher temperature difference, approximately 335 K to 330 K, representing the effect of higher water velocity on heat transfer. Also, for V1 = 0.1 m/s and V2 = 0.5 m/s, the temperature at point 4 starts at 295 K and rises to about 300 K, which is not very large. This comparison shows that inlet velocities have a tremendous impact on temperature profiles at point 4; an increase in water velocities results in better heat transfer and faster attainment of thermal equilibrium.



**Figure 20:** Comparison of temperature distribution for all cases ((V1=0.1, V2=0.3 m/s), (V1=0.3, V2=0.1 m/s))

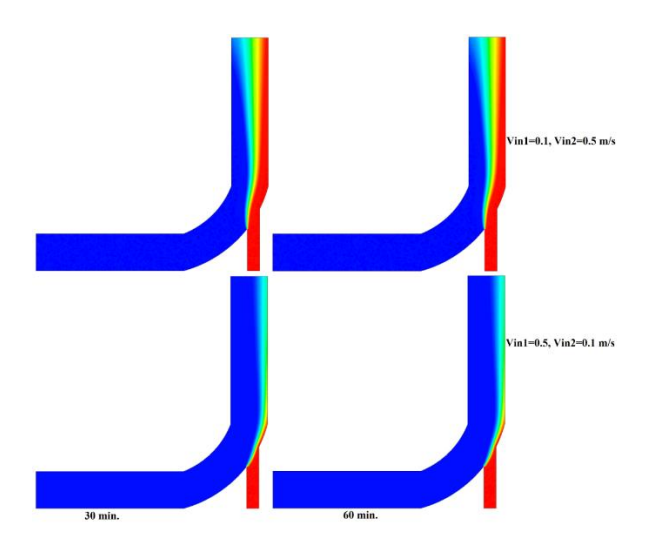


Figure 21: Comparison of temperature distribution for all cases ((V1=0.1, V2=0.5 m/s), (V1=0.5, V2=0.1 m/s))

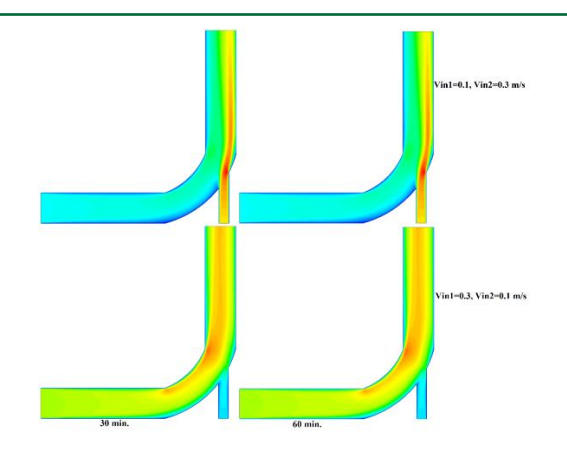


Figure 22: Comparison of velocity distribution for all cases ((V1=0.1, V2=0.3 m/s), (V1=0.3, V2=0.1 m/s))

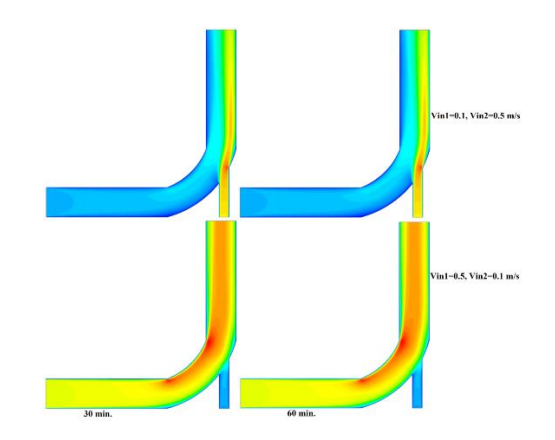
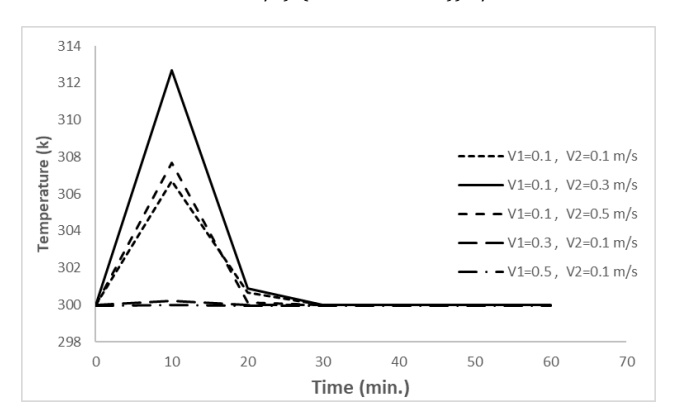
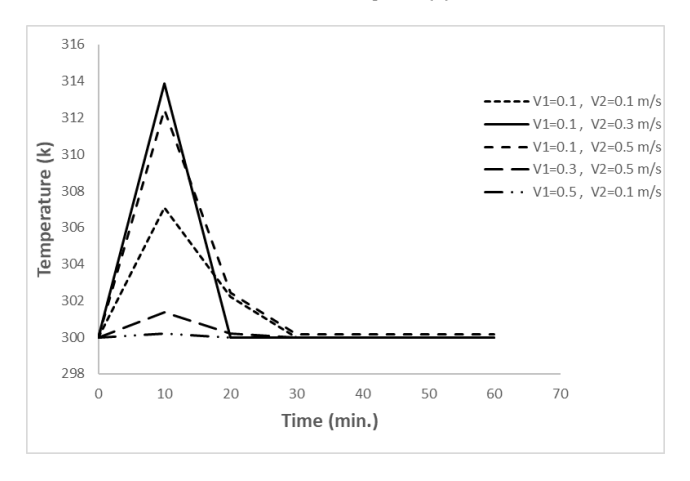


Figure 23: Comparison of velocity distribution for all cases ((V1=0.1, V2=0.5 m/s), (V1=0.5, V2=0.1))m/s



**Figure 24:** Comparison of temperature distribution for all cases in point (1)



**Figure 25:** Comparison of temperature distribution for all cases in point (2)

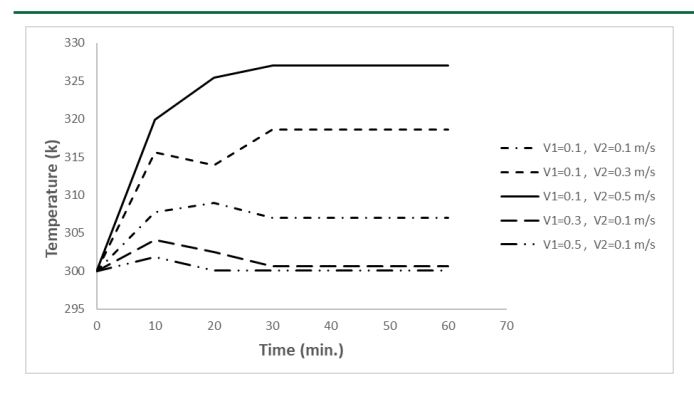


**Figure 26:** Comparison of temperature distribution for all cases in point (3)

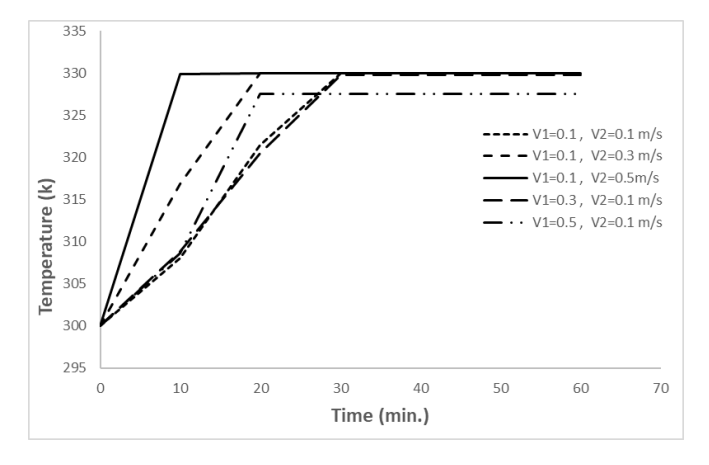


**Figure 27:** Comparison of temperature distribution for all cases in point (4)

#### 4. CONCLUSIONS

The primary area of concern of this research was to compare the thermal and velocity distribution of a fluid system with different approaches at the inlet velocities. The goal was to investigate how several variables of water and air velocities altered temperature distributions at various positions within the system to gain knowledge for improved efficiency in applications of thermal management in engineering. From this paper, we can deduce the following conclusions:

- The study confirmed that higher water and air inlet velocities improve heat transfer efficiency. For instance, at point 1, the temperature increased from 298 K to 300 K for V1 = 0.1 m/s, V2 = 0.1 m/s, while for V1 = 0.5 m/s, V2 = 0.1 m/s, the temperature rose from 335 K to 330 K, demonstrating a more effective thermal transfer at higher water velocities.
- Higher air velocities facilitated better temperature uniformity. At point 2, when V1 = 0.1 m/s and V2 = 0.3 m/s, the temperature increased from 296 K to 302 K, confirming that increased air velocity enhances heat distribution across the chamber.
- Velocity contours showed that higher water inlet velocities promoted more uniform flow. For V1 = 0.5 m/s, V2 = 0.1 m/s, the velocity near the water inlet was 0.5 m/s, whereas at the air inlet, it was 0.1 m/s, leading to a more stable velocity field and improved fluid mixing.
- The case with V1 = 0.3 m/s and V2 = 0.1 m/s resulted in a faster temperature rise to 315 K, while in V1 = 0.1 m/s and V2 = 0.1 m/s, the temperature rise was only 300 K, highlighting the advantage of increased water velocity in accelerating thermal mixing.
- The study demonstrated that higher water velocities (V1 = 0.5 m/s) resulted in faster temperature stabilization at 330 K, whereas lower velocities required longer mixing times and less uniform temperature

distribution, emphasizing the role of optimized inlet velocity settings.

 These findings provide a foundation for optimizing thermal management in heat exchangers, chemical reactors, and environmental control systems. Future research should explore additional parameters, such as chamber geometry modifications and different working fluids, to further enhance mixing efficiency.

#### **REFERENCES**

- Al-Naqqash, H.R., Mohammed Alhwayzee et al., 2024. Simulating the Rising Air Bubbles Stream Through Heavy Fuel Oil Residue Bubble Column Reactor using COMSOL. Journal of Advanced Research in Fluid Mechanics and Thermal Sciences, 2024. 121 (1): Pp. 70-84. https://doi. Org/10.37934/arfmts.121.1.7.
- Bhatkar, V. W., and Sur, A., 2021.An experimental analysis of liquid air jet pump. Frontiers in Heat and Mass Transfer, 2021. 17(12): Pp. 1-5.
- Devos, C., Mukherjee, S., Inguva, P., Singh, S., Wei, Y., Mondal, S., and Myerson, A. S., 2025. Impinging jet mixers: A review of their mixing characteristics, performance considerations, and applications. AIChE Journal, 2024: Pp. e18595.
- Esfarjani, S.A., and Dolatabadi, A., 2009. A 3D simulation of two-phase flow in an effervescent atomizer for suspension plasma spray. Surface and Coatings Technology, 2009. 203(15): Pp. 2074-2080.
- Ferreira, G., Barreras, F., Lozano, A., Garcia, J. A., and Lincheta, E., 2009. Effect of the inner two-phase flow on the performance of an industrial twin-fluid nozzle with an internal mixing chamber. Atomization and Sprays, 2009. 19(9).
- Herringe, R.t., and Davis, M., 1976. Structural development of gas-liquid mixture flows. Journal of Fluid Mechanics, 1976. 73(1): Pp. 97-123.
- Jing, Q., Xu, W., Ye, W., and Li, Z., 2022. The Relationship between Contraction of the Ejector Mixing Chamber and Supersonic Jet Mixing Layer Development. Aerospace, 2022. 9(9): Pp. 469.
- Khalaf, A. F., Rashid, F. L., Mohammed, H. I., Basem, A., Rasool, H., and Al-Obaidi, M. A., 2024. Numerical Unveiling the Dynamics of Glycerin-Water Mixing: Insights into Compatibility and Behavior. Journal of Advanced Research in Numerical Heat Transfer, 2024. 16(1): Pp. 35-56
- Khalaf, A. F., Rashid, F. L., Mohammed, H. I., Basem, A., Rasool, H., and Al-Obaidi, M. A., 2024. Numerical Unveiling the Dynamics of Glycerin-Water Mixing: Insights into Compatibility and Behavior. Journal of Advanced Research in Numerical Heat Transfer, 2024. 16 (1): 34-55. https://doi.org/10.37934/arnht.16.1.3455.
- Lefebvre, A., 1988. A novel method of atomization with potential gas turbine applications. Defence Science Journal, 1988. 38(4): Pp. 353-362.
- Li, X., Santos, R. J., and Lopes, J. C. B., 2007. ModellingModelling of self-induced oscillations in the mixing head of a rim machine. The Canadian Journal of Chemical Engineering, 2007. 85(1): Pp. 45-54.
- Mehmood, K. and Masud, J., 2012. Analysis of two-phase flow in an effervescent atomizer using volume of fluid method. in 50th AIAA aerospace sciences meeting including the new horizons forum and aerospace exposition.
- Rashid, F. L., Al-Obaidi, M. A., Hussein, A. K., Ahmad, S., Albdeiri, M. S., and Mujtaba, I. M., 2024. Bubble Dynamics in Sustainable Technologies: A Review of Growth, Collapse, and Heat Transfer. Processes, 2025. 13(38). https://doi.org/10.3390/pr13010038.
- Shao, C., Zhong, G., and Zhou, J., 2021. Study on gas-liquid two-phase flow in the suction chamber of a centrifugal pump and its dimensionless

- characteristics. Nuclear Engineering and Design, 2021. 380: p. 111298.
- Sheha, A. A. A., Ibrahim, K. A., Abdalla, H. A., El-Behery, S. M., and Sakr, I. M., 2024.improvement of the axial-jet-pump performance using modified mixing chamber configuration and inlet swirling flow. Scientia Iranica, 2024. 31(1): p. 26-42.
- Sliusenko, A., Ponomarenko, V., and Forostiuk, I., Water-air ejector with conical-cylindrical mixing chamber. 2021.
- Tian, M., Edwards, J., Lin, K. C., and Jackson, T., 2003. Numerical simulation of transient two-phase flow with aerated liquid injectors. Part 2: flow structure. in 33rd AIAA fluid dynamics conference and

exhibit.

- Vojkůvková, P., Šikula, O., and Weyr, J., 2015. Assessment of condensation of water vapor in the mixing chamber by CFD method. in EPJ Web of Conferences. 2015. EDP Sciences.
- Wang, R. H., Du, Y. K., Ni, H. J., and Lin, M. A., 2011. Hydrodynamic analysis of suck-in pulsed jet in well drilling. Journal of Hydrodynamics, Ser. B, 2011. 23(1): Pp. 34-41.
- Zhang, Y., Gerdroodbary, M. B., Hosseini, S., Abazari, A. M., and Li, Z., 2021.Effect of hybrid coaxial air and hydrogen jets on fuel mixing at supersonic crossflow. International Journal of Hydrogen Energy, 2021. 46(29): Pp. 16048-16062.

